Porous activated carbon materials from Triphala seed stones for high-performance supercapacitor applications

Chhabi Lal Gnawali[1,*]**, Sabina Shahi**[2]**, Sarita Manandhar**[3]**, Ganesh Kumar Shrestha**[1]**, Mandira Pradhannanga Adhikari**[2]**, Rinita Rajbhandari**[1]**, Bhadra P. Pokharel**[1]

[1]*Department of Applied Sciences and Chemical Engineering, Pulchowk Campus, Institute of Engineering (IOE), Tribhuvan University, Lalitpur, Nepal*
[2]*Central Department of Chemistry, Tribhuvan University, Kirtipur, Kathmandu, Nepal*
[3]*Tri-Chandra Multiple Campus, Kathmandu, Nepal*
*Corresponding author. Email: chhabig123@ioe.edu.np

Abstract

Porous activated carbon materials derived from biomass could be the suitable materials for high-rate performance electrochemical supercapacitors as it exhibits high surface area due to the development of nanopores. Here, we report the novel porous activated carbon from Triphala seed stones by chemical activation with zinc chloride at different carbonization temperature (400-700 ^0C) under the nitrogen gas atmosphere. The activated carbon was characterized by Fourier transform-infrared (FTIR) spectroscopy, Raman scattering and scanning electron microscopy (SEM). Nitrogen adsorption-desorption measurements was used to study the surface properties (effective surface areas, pore volumes and pore size distributions). The electrochemical measurements were performed in an aqueous 1 M sulphuric acid (H_2SO_4) solution in a three-electrode cell set up. The specific surface area of Triphala seed stones-derived porous carbon materials with well-defined micro- and mesopores ranges from 878.7 to 1233.3 m^2 g^{-1} and total pore volume ranges from 0.439 to 0.626 cm^3 g^{-1}. The specific capacitance obtained by electrochemical measurement experiment was 208.7 F g^{-1} at 1 A g^{-1}. These results indicate that the prepared nanoporous activated carbon material from Triphala seed stones would have significant possibility as supercapacitor electrode material for high-energy-storage supercapacitor applications.

1 Introduction

In 21st century, because of urbanization, industrialization as well as the rapid growth of population, the energy storage and the environmental pollution are considered thoughtful challenges worldwide. The continuous depletion of fossil fuel, climate change due to excessive greenhouse gases, high energy cost leads the society towards renewable as well sustainable energy sources so it is essential to develop the sustainable energy storage system with high power density and energy density. Nowadays, the electrochemical energy storage systems like lithium-ion batteries, fuel cells, solar cells, supercapacitors are widely used in electronics and electrical vehicles [1–4]. So, researchers have keen interest on supercapacitors with ultra-high power density, fast charging discharging rates, superior cycle life, low internal resistance, environment friendly, low cost, safe and easy operations [5–8].

Supercapacitors, also known as electrical double-layer capacitors (EDLCs), store charges at the surface of electrode material by means of electrical double layers via electrolyte-ion diffusion from electrolyte solution to the electrode. The performance of supercapacitors depends upon the electrode material. The carbon black, carbon nanotubes, glassy carbon, activated carbon-the carbon-based materials and the transition metals are commonly used for electrode materials [9]. In general, the commercial activated carbons prepared from fossil fuel-based precursors which are nonrenewable, expensive and environmentally non-friendly hence the researchers have great interest to prepare the activated carbon from the lignocellulosic materials. The biomass precursors are renewable, cheaper, easily available, environment friendly and highly porous materials. Because of high specific surface area, well-developed pore size distributions, nanoporous activated carbons can be used as the suitable material for the supercapacitors to increase the specific capacitance [10–12]. In recent years, researchers have used various biomass materials and industrial wastes like lapsi seed, argan seed, peanut shell, sugarcane bagasse, wheat husk, etc. [13–19] as a raw material for the preparation of nanoporous activated carbon that can be used in the waste water treatment as well as the energy applications. They are renewable, locally available resources in large quantities as well as cost efficient and eco-friendly.

Triphala is well recognized polyherbal medicine comprises Harro (*Terminalia Chebula*), Barro (*Terminalia bellirica*), and *Amala (Phyllanthus emblica)* have found potentially effective in Ayurvedic medicine and even used for treating and preventing from cancer [20,21]. However, no research work

observed on Triphala seed stones for the preparation of activated carbon but Phyllanthus emblica seed-derived hierarchically porous carbon materials for supercapacitor applications is recently reported [22]. Because of being the pillar of Ayurvedic medicine, biomass materials, low cost which are locally available in different regions of Nepal, there is particular interest towards the study of preparing a nanoporous carbon material from Triphala seed stones.

In this contribution, we report the production of AC from Triphala seed stones by chemical activation method using zinc chloride as an activating agent to study the performance of supercapacitor. The Triphala seed powder was mixed with zinc chloride in 1:1 weight ratio and carbonized at different temperatures (400, 500, 600 and 700 ^{0}C) for 4 hours under the constant flow of ultrapure nitrogen gas. Thus, prepared AC materials were named on the basis of carbonization temperature as MxC-Z400, MxC-Z500, MxC-Z600 and MxC-Z700 respectively. The control sample is prepared by direct carbonization at 500 ^{0}C and named as MxP-500. Raman spectroscopy, Fourier-transform infrared (FTIR) spectroscopy, scanning electron microscopy (SEM), and nitrogen adsorption/desorption isotherms are used to characterize the prepared activated carbons. The electrochemical energy-storage supercapacitance performance of the novel nanoporus activated carbon prepared from Triphala seed stones by $ZnCl_2$ activation also reported. The obtained AC shows high surface area 1233.3 m^2g^{-1}, and pore volume 0.626 cm^3g^{-1} achieving excellent specific capacitance of 208.7 F g^{-1} at 1 A g^{-1}. These results indicate that Triphala seed, a Bio-waste material, has the potential for the production of porous carbon materials to improve the performance of supercapacitors and may be useful to control the energy crisis in Nepal.

2 Materials and Methods

2.1 Preparation of activated carbon

The samples acquired from local vendors were peeled and seed stone separation was done. The obtained seed stones were cleaned with distilled water several times before drying in an oven for 24 hours at 50 ^{0}C. After that, the seed stones were mechanically broken into powder and sieved through a mesh size of 300 μm for the precursor. The MxP-500, the control sample refers to directly carbonized carbon that was synthesized in a tube furnace under an inert atmosphere of nitrogen gas for four hours at 500 ^{0}C.

The activated carbon was prepared through chemical activation using $ZnCl_2$ as an activating agent in 1:1 ratio on the powder precursor, and the

effects of different carbonization temperature (400, 500, 600, and 700 ^{0}C) were investigated. The carbonization process was carried out in a tube furnace (Accumax India) with a constant supply of nitrogen gas. After cooling, the carbonized products were treated with 5 % HCl and then with distilled water until the supernatant liquid reached a pH of 7, and then dried at 100^0C for three hours. The activated carbons prepared at carbonization temperatures 400, 500, 600, and 700 0C were labeled as MxC-Z400, MxC-Z500, MxC-Z600, and MxC-Z700, respectively.

2.2 Characterizations of Triphala seed-derived carbon materials

The surface area and textural properties of the mixture precursor powder and the activated porous carbon materials were investigated by different methods. Precursor powder was subjected to a thermogravimetric analysis (TGA) on a SII instrument (Model Exstar 600) from 25 to 1000^0C with a temperature ramp of 10 ^{0}C min^{-1} in a nitrogen gas atmosphere. Raman spectroscopy (NRS-3100, JASCO, Tokyo, Japan), Fourier-transform infrared (FTIR) spectroscopy (Nicolet 4700, Thermo Electron Corporation, Waltham, MA, USA), scanning electron microscopy (SEM: S-4800, Hitachi Co., Ltd. Tokyo, Japan operated at 10 kV) and nitrogen adsorption/desorption isotherms (Quantachrome Autosorb-iQ2, Boynton Beach, FL, USA) were used for instrumental characterization. The nitrogen adsorption/desorption isotherms estimated the total pore volume, pore size distribution, and specific surface area. Using Barrett-Joyner-Halenda (BJH) and density functional theory (DFT) method, pore diameters and volumes were determined. For nitrogen adsorption isotherm, about 35 mg of sample was placed in a glass cell and degassed at 120 ^{0}C for 24 hrs before recordings.

2.3 Electrochemical supercapacitance performance studies

The electrochemical supercapacitance of Triphala seed-derived activated carbon was studied by using cyclic voltammetry (CV), galvanostatic charge/discharge (GCD), and electrochemical-impedance-spectroscopy (EIS) measurements in a three-electrode-cell set-up in aqueous 1 M H_2SO_4 electrolyte solution. The glassy-carbon electrode (GCE) was used as the working electrode. The fine carbon powder was added to a mixture of water and ethanol (2 mL: 4:1 v/v ratio) and sonicated for 60 min to obtain a dispersion of carbon (2 mg mL^{-1}. Certain volume of the suspension (3 µL) was dropped on a clean and dry GCE, and dried at 60^0C for 2 hrs to solvent evaporation. The mass of the active electrode-material for each system was 3

$\times$ 10^{-6} g. Nafion solution (5 μL: 5% in ethanol) was used as the binder, after that the working electrode was dried at 80 ^{0}C for 2 hrs under vacuum. The CV, GCD, and EIS measurements were performed on a CHI 660E workstation (CH Instruments, Inc. Austin, TX, USA) by taking Platinum wire as the counter electrode, and Ag/AgCl as the reference electrode. The GCD curves obtained from the chronopotentiometry measurements is used to calculate the specific capacitance (Cs) of the electrode materials as

$$C_s = \frac{I \times t_d}{m \times \Delta V} \qquad (1)$$

where, I (A) indicate the discharge current, t_d(s) is the discharge time, m (g) is the mass of active material on the GCE electrode and (V) represent the operating voltage.

3 Results and Discussion

3.1 TGA and FTIR analysis

The pyrolytic seed decomposition of mixture seed powder was studied by thermogravimetric analysis. The TGA curve in figure 1a shows the recording from 25 to 1000 ^{0}C under nitrogen gas atmosphere that indicates the pyrolysis process of precursor occurred in three stages. In the first stage, weight loss happens as a result of evaporation of moisture being locked in the sample at temperatures below 250 ^{0}C. At the second stage, there is a significant weight loss between 250 and 370 ^{0}C, which is caused by the pyrolytic destruction of the cellulose and hemicellulose components along with partial decomposition of the lignin content. Precursor slowly breaks down into carbon components in the third stage; hence there is no considerable weight loss above 370 ^{0}C. FTIR analysis of powder (figure 1b) indicates the presence of several oxygenated surface functional groups of precursors corresponding to cellulose, hemicellulose and lignin. A broad FTIR peak at 3337 cm^{-1} relates to the O–H stretching (str.) of the moisture water and/or alcoholic group of the cellulose. At the same time, bands at 2929 and 2850 cm^{-1} denote the cellulose's aliphatic C-H (str.). The band at 1730 cm^{-1} corresponds to the unsaturated ester's C=O (str.) [23]. In addition, the absorption band at 1587 and 1229 cm^{-1} arise from the aromatic C=C stretching and the C–O stretching in lignin, respectively. The band at 1322 cm^{-1} can be associated with the C-H symmetric deformation that is typical in cellulose and hemicelluloses [24, 25]. The bands in the regions 1028 cm^{-1} are due to alkoxy C-O (str.) or other C-O (str.) in cellulose, hemicellulose or lignin. Due to the high temperature carbonizations, the FTIR bands corresponding to the oxygenated surface functional group in the ZnCl$_2$ activated carbon samples substantially diminished [26].
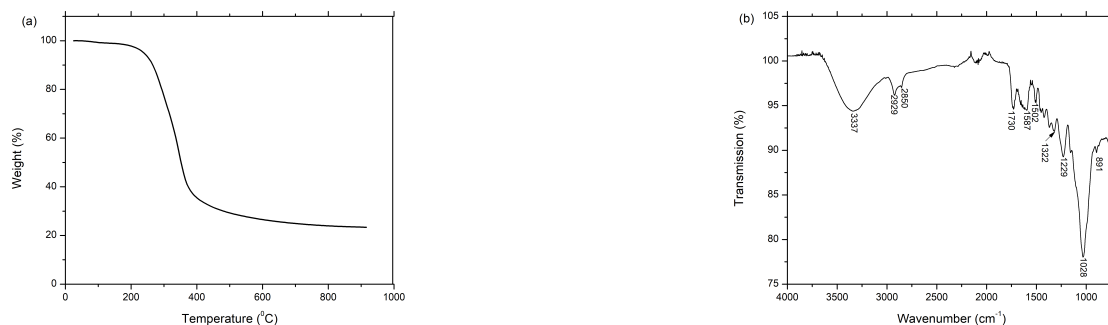
Figure 1: (a) TGA curve of Triphala seed powder (precursor); (b) corresponding FTIR spectrum.

3.2 Nitrogen adsorption desorption isotherm

By using nitrogen adsorption desorption isothermometry, the surface textural characteristics of produced carbon samples were investigated. The adsorption isotherm of carbons activated at various temperatures is shown in Figure 2a. All of the carbon materials showed higher nitrogen adsorption at low relative pressures and significant hysteresis at high relative pressures. These isotherms combine type I and type IV, which suggests that the micro- and mesopore structures are hierarchical [27]. High nitrogen uptake may be attributed to the filling of micropores at low relative pressures (P/P0), but the hysteresis loop in the region of high relative pressures may be caused by capillary condensation taking place in the mesopores. While nitrogen uptake at low relative pressure appeared to increase, the integral area of the hysteresis loop decreased as carbonization temperature increased from 400 to 700 ^{0}C, indicating that there were more micropores present at higher temperatures and fewer mesopores in the carbon framework. Large surface areas offered by these micro- and mesopore structures facilitate dye molecule dispersion on the carbon surface during adsorption [28]. The pore size distribution curves obtained by DFT and BJH analysis is shown in figure 2b and 2c respectively. Table 1 provides a summary of the surface textural properties of ZnCl$_2$-activated Triphala seed carbon as determined by nitrogen adsorption experiments.

3.3 Raman spectra

The image displays two distinct Raman bands in the spectra. The defect or disordered phase of carbon may be responsible for the first peak (D-band) at 1350 cm^{-1} and the graphitic phase of carbon may be responsible for the second peak (G-band) at 1598 cm^{-1} . Although the G-band reflects the stretching vibration of sp^2 hybridized carbon atoms in the graphitic layer, the D-band represents the vibration of sp^3 hybridized carbon atoms in disordered graphitic structure [29].

Table 1: Surface textural properties of Triphala seed carbon at different carbonization temperature (SSA=total specific surface area, Smic=micropore surface area, Smes=mesopore surface area, Vp=total pore volume, Vmic=micropore volume, Vmes=mesopore volume, WH=average half-pore width of micropores, Dp=average pore diameter of mesopores)

System	SSA(m^2/g)	Smic(m^2/g)	Smes(m^2/g)	Vp(cc/g)	Vmic(cc/g)	Vmes(cc/g)	WH (nm)	Dp(nm)
MxC-Z400	1137.7	1087.2	50.5	0.6	0.54	0.06	0.286	3.66
MxC-Z500	1233.3	1195.1	38.2	0.626	0.574	0.052	0.286	3.66
MxC-Z600	1143.8	1082.7	61.1	0.617	0.537	0.08	0.286	3.66
MxC-Z700	878.7	836.9	41.8	0.439	0.384	0.055	0.286	3.67
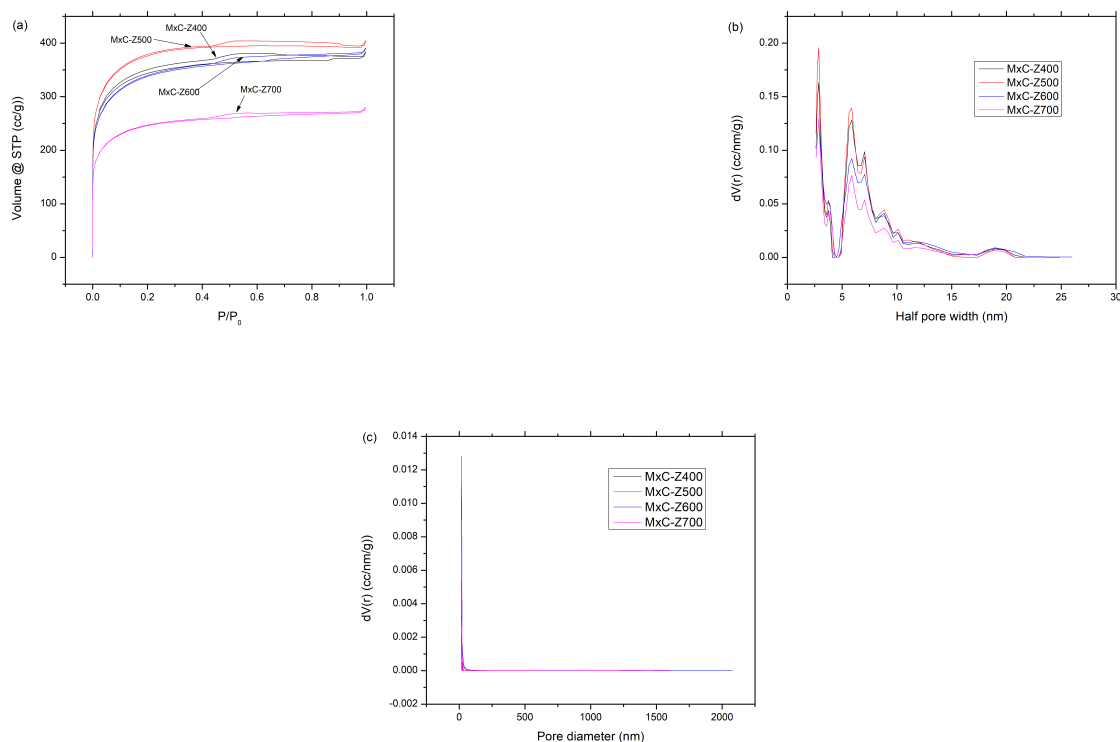
Figure 2: (a)Nitrogen adsorption-desorption isotherms of the carbon samples, (b) pore size distributions calculated using the DFT method and (c) pore size distributions calculated from the BJH method

The degree of graphitization of carbon materials is estimated by the help of ratio of the intensities of the G and D bands (I_G/I_D). Decreasing crystallinity is indicated by an increase in the I_G/I_D ratio. The produced carbon samples exhibit I_G/I_D ratios between 1.05 and 1.29, which point to the development of amorphous graphitic carbon with few structural defects. As the carbonization temperature is raised from 400 to 700 ^{C}, the I_G/I_D ratio falls from 1.15 to 1.05, indicating an increase in graphitic carbon. Electrical conductivity, specific area, and pore size are all impacted by the degree of graphitic structure, which impact on increasing the performance of the supercapacitor electrode [22].

3.4 SEM analysis

The surface morphology of the mixture seed carbons was investigated using SEM images. SEM images show irregularly shaped and sized pore structure with microporous channels on their surfaces. Most carbon particles are between a range of few and several tens of microns in size. The MxP-500 has very less surface porosity (Figure 4a-b) which in agreement with nitrogen sorption data. The mesopore structure of MxP-500 is hardly visible in the high-resolution SEM image (Figure 4b). The ZnCl$_2$ activation results increases the surface

porosity (Figure 4d, f, g, h, i, j). The nitrogen adsorption isotherm results correspond with the SEM pictures of the ZnCl$_{2-}$ activated samples, which show a large number of macroporous channel-like structures whose frameworks comprise of micro/mesopores, indicating the formation of hierarchical pore structures. While mesopores are numerous, micropores are not easily visible in the ZnCl$_{2-}$ activated samples (Figure 4d, f, g, h, i, j).

3.5 Electrochemical measurements

The high surface area and the hierarchically porous structure of the prepared sample motivate to calculate the supercapacitance performance. The comparison of CV profiles of MxP-500, MxC-Z400, MxC-Z500, MxC-Z600 and MxC-Z700 performed at 50 mVs^{-1} is shown in figure 5a. The quasi-rectangular profiles of all the samples exhibit the EDLC-type energy storage mechanism. The weak redox peaks at 0.2-0.4 V for MxC-Z400 CV curve indicate the partial contribution of pseudocapacitance to the EDLC because of presence of the oxygen functionalities in the carbon material [22]. The low value of total internal current of CV curve in MxP-500 sample is due to the lack of porosity. The current output of the MxC-Z700 sample is higher which indicates the sample MxC-Z700 stored the
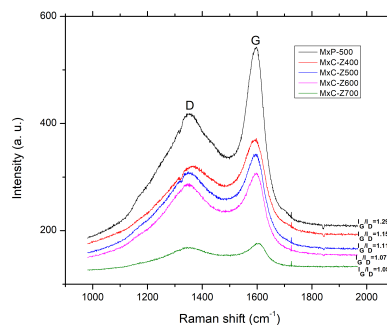
Figure 3: Raman scattering spectra of MxP-500, MxC-Z400, MxC-Z500, MxC-Z600, and MxC-Z700.
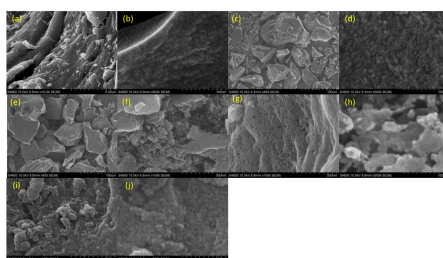
Figure 4: SEM images of (a, b) MxP-500; (c, d) MxC-Z400; (e, f) MxC-Z500; (g, h) MxC-Z600; and (i, j) MxC-Z700.

highest energy among all the samples.

By using Galvano-static charge-discharge (GCD) at different current densities (1, 2, 3, 4, 5, 10, 20, 30, 40, 50 A g^{-1}), the electrochemical charge storage mechanism was studied. Figure 6a shows the GCD profiles of all the samples at 1 A g^{-1}, including the reference carbon, which are of triangular form confirming an EDLC-type charge storage mechanism. From the above result, we see that the reference sample MxP-500 shows the lowest charge discharge time whereas the MxC-Z700 shows the highest charge discharge time which confirms the maximum charge storage capacity because of the nanoporous structure [30–32]. The GCD curves of all the samples have the triangular form and remains even at high current density of 50 A g^{-1}), that confirm the effective ion diffusion mechanism at interiors of the nanoporous carbon materials at higher current densities. Figure 6e shows the specific capacitance as the function of current density for all the samples. From this graph, we see that the specific capacitance of direct carbonized sample is very low as expected because of its low porosity while that of MxC-Z700 is superior at all current densities from 1 to 50 A g^{-1}. The specific capacitance was calculated by using equation (1).

To investigate the diffusion kinetics of the electrolyte ions, electron-transfer resistance and double-layer charging at the electrode-electrolyte interface, the electrochemical impedance spectroscopy (EIS) was conducted [33]. Figure 7 shows the Nyquist plot of prepared nanoporous activated carbon materials. The plots of $ZnCl_2$ activated carbon samples shows the lack of semicircular component indicating ideal EDLC type charge transfer. The steep rise in the low frequency region indicates the rapid ion transfer in the electrode. The series resistance of the electrode is given by the x-axis intercept of the imaginary component of impedance, which is close to 4.9 Ω for the activated carbon. This low value of series resistance confirms the importance of interconnected nanoporous structure to increase conductivity during ion transfer and almost similar for all carbon samples, which indicates the surface-textural properties governed the energy-storage capacity of the electrodes.

4   Conclusion

In conclusion, we have successfully synthesized nanoporous activated carbon materials from novel material, Triphala (*Terminalia chebula, Terminalia bellirica, and Phyllanthus emblica*) by chemical activation with zinc chloride ($ZnCl_2$) at different carbonization temperatures (400, 500, 600 and 700 ^{0}C). Surface textural properties show that the carbonization temperature play the significant role on porosity. The surface area of the prepared novel carbon materials from Triphala ranges from 878.7 to 1233.3 m^2 g^{-1} and the pore volume ranges from 0.439 to 0.626 cm^3 g^{-1}. Also, we have studied the electrochemical supercapaci-
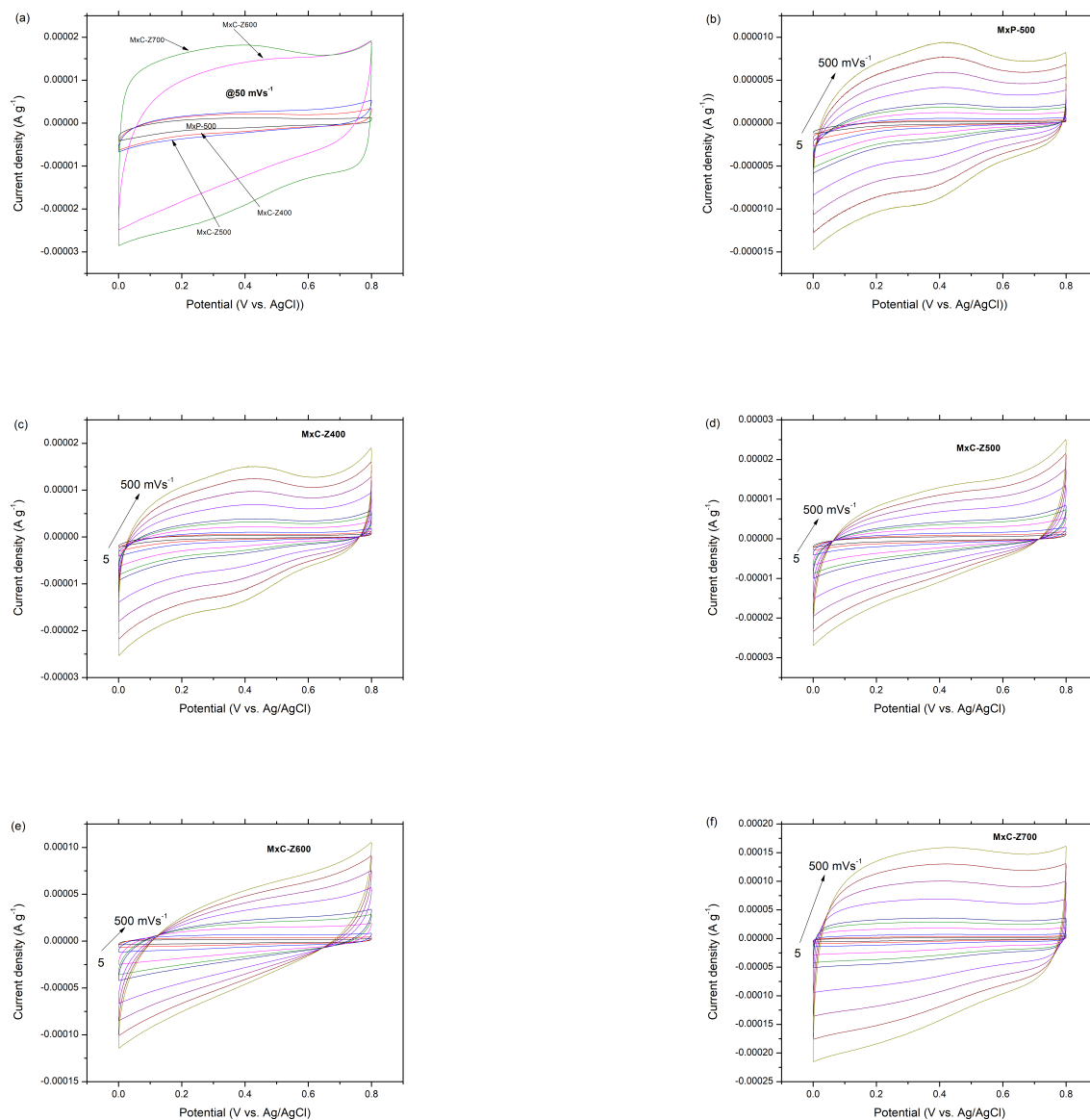
Figure 5: Electrochemical -energy-storage performance by CV measurements: (a) CV curves at fixed potential sweep of 50 mVs^{-1}; and CV curves at various sweep-rates (5, 10, 20, 50, 80, 100, 200, 300, 400 and 500 mVs^{-1}) for (b) MxP-500; (c) MxC-Z400; (d) MxC-Z500; (e) MxC-Z600; (f) MxC-Z700
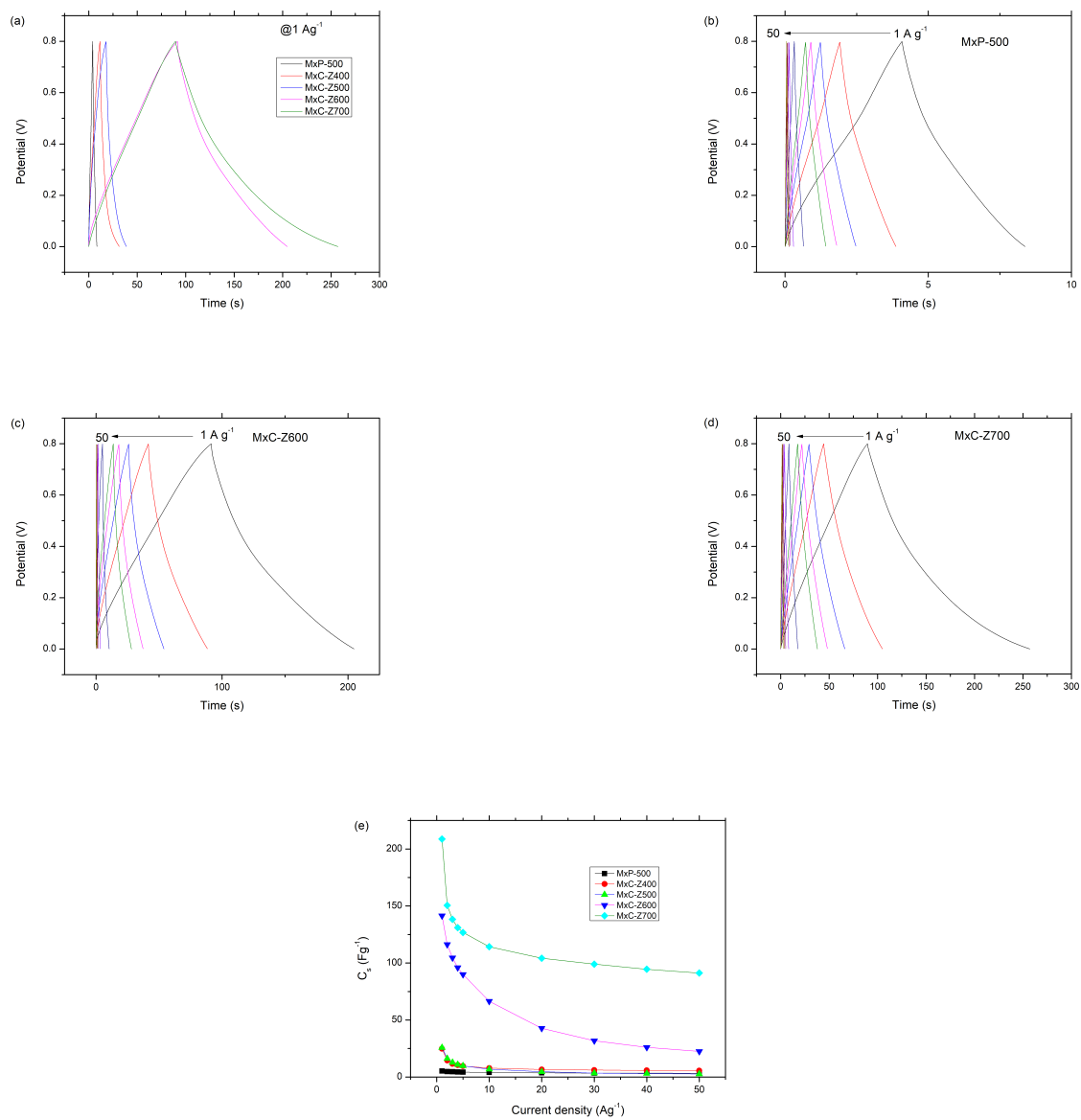
Figure 6: (a) GCD profiles of all the samples at current density of 1 A g-1, CD curve of (b) MxP-500, (c) MxC-Z600, (d), MxC-Z700 at different current densities from 1 to 50 A g^{-1} and (e) specific capacitance as a function of current density for all samples.
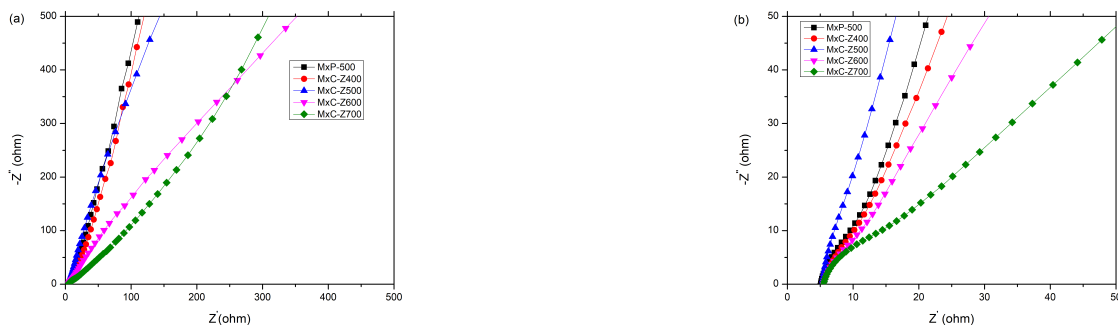
Figure 7: EIS Results: (a) Nyquist plots of different carbon materials (MxP-500, MxC-Z400, MxC-Z500, MxC-Z600 and MxC-Z700) in 1 M H_2SO_4 electrolyte from 0.01 Hz to 100 kHz at an amplitude of 5 mV (b) the corresponding magnified plot.

tance performance of the prepared nanoporous activated carbon in aqueous electrolyte (1 M H_2SO_4) in a three-electrode system. Because of their large surface area, large pore volume and interconnected mesopore structure, the prepared sample exhibit the excellence specific capacitance of 208.7 F g^{-1} at 1 A g^{-1}. From these results we can conclude that the bio-waste material like Triphala seed stones could be the potential source for the preparation of nanoporous activated carbon that will be suitable for the preparation of electrode material for high performance energy-storage supercapacitors.

Acknowledgement

References

[1] A. Elmouwahidi, Z. Zapata-Benabithe, F. Carrasco-Marin, and C. Mareno-Castilla. Activated carbon from koh-activation of argan (argania spinosa) seed shells as supercapacitor electrodes. *Bioresource Technology*, 111:185–190, 2012.

[2] R. G. Shrestha, L. K. Shrestha, and K. Ariga. Carbon nanoarchitectinics for energy and related applications. *CJ. Carbon Res.*, 7:73, 2021.

[3] L. K. Shrestha, R. G. Shrestha, S. Shahi, C. L. Gnawali, M. P. Adhikari, B. N. Bhadra, and K. Ariga. Biomass nanoarchitectonics for supercapacitor applications. *J. Oleo Sci.*, 72(1):11–32, 2023.

[4] R. Rajbhandari, L. K. Shrestha, B. P. Pokharel, and R. R. Pradhananga. Development of nanoporous structure in carbons by chemical activation with zinc chloride. *Journal of Nanoscience and Nanotechnology*, 13:2613–2623, 2013.

[5] M. Shi, Y. Xin, X. Chen, K. Zou, W. Jing, J. Sun, and Y. Chen. Coal-derived porous activated carbon with ultrahigh specific surface area and excellent electrochemical performance for supercapacitors. *Journal of Alloys and Compounds*, 859:157856, 2021.

[6] E. Elaiyappillai, R. Srinivasan, Y. Johnbosco, P. Devakumar, K. Murugesan, K. Kesavan, and P. M. Johnson. Low cost activated carbon derived from cucumis melo fruit peel for electrochemical supercapacitor application. *Applied Surface Science*, 486:527–538, 2019.

[7] S. Sundriyal, V. Shrivastav, H. D. Pham, S. Mishra, A. Deep, and D. P. Dubal. Advances in bio-waste derived activated carbon for supercapacitors: Trends, challenges and prospective. *Resources, Conservation & Recycling*, 169:105548, 2021.

[8] R. L. Shrestha, R. Chaudhary, R. G. Shrestha, T. Shrestha, S. Maji, K. Ariga, and L. K. Shrestha. Washnut seed-derived ultrahigh surface area nanoporous carbons as high rate performance electrode material for supercapacitors. *Bulletin of the Chemical Society of Japan*, 94:565–572, 2021.

[9] A. M Abioye and F. N. Ani. Recent development in the production of activated carbon electrodes from agricultural waste biomass for supercapacitors: A review. *Renewable and Sustainable Energy Reviews*, 52:1282–1293, 2015.

[10] M. M. M. Ahmed, T. Imae, H. Ohshima, k. Ariga, and L. K. Shrestha. External magnetic field-enhanced supercapacitor performance of cobalt oxide/magnetic graphene composites. *Bulletin of the Chemical Society of Japan*, 94:2245–2251, 2021.

[11] R. Chaudhary, S. Maji, R. G. Shrestha, R. L. Shrestha, T. Shrestha, K. Ariga, and L. K. Shrestha. Jackfruit seed-derived nanoporous carbon as the electrode material for supercapacitors. *C Journal of Carbon Research*, 6:73, 2020.

[12] R. L. Shrestha, R. Chaudhary, T. Shrestha, B. M. Tamrakar, R. G. Shrestha, S. Maji, J. P. Hill, K. Ariga, and L. K. Shrestha. Nanoarchitectonics of lotus seed derived nanoporous carbon materials for supercapacitor applications. *Materials*, 13:5434, 2020.

[13] L.K. Shrestha, R.G. Shrestha, S. Maji, B.P. Pokharel, R. Rajbhandari, R.L. Shrestha, R.R. Pradhananga, J.P. Hill, and K. Ariga. High surface area nanoporous graphitic carbon materials derived from lapsi seed with enhanced supercapacitance. *Nanomaterials*, 10(4):728, 2020.

[14] S. Joshi, L.K. Shrestha, Y. Kamachi, V. Malgras, M.A. Pradhananga, B.P. Pokharel, T. Naata, R.R. Pradhananga, K. Ariga, and Y. Yamauchi. Synthesis and characterizations of nanoporous carbon derived from lapsi (choerospondias axillaris) seed: Effect of carbonization conditions. *Advances in Powder Technology*, 26(3):894–900, 2015.

[15] A. Elmouwahidi, Z. Zapata-Benabithe, F. Carrasco-Marin, and C. Mareno-Castilla. Activated carbon from koh-activation of argan (argania spinosa) seed shells as supercapacitor electrodes. *Bioresource Technology*, 111:185–190, 2012.

[16] Y. Zhan, H. Zhou, F. Guo, B. Tian, S. Du, Y. Dong, and L. Qian. Preparation of highly porous activated carbon from peanut shells as low-cost electrode materials for supercapacitors. *Journal of Energy Storage*, 34:102180, 2021.

[17] T.E. Rufford, D. Hulicova-Jurcakova, K. Khosla, Z. Zhu, and G.Q. Lu. Microstructure and electrochemical double-layer capacitance of carbon electrodes prepared by zinc chloride activation sugar cane bagasse. *Journal of Power Sources*, 195(3):912–918, 2010.

[18] M.M. Baig and I.H. Gul. Conversion of wheat husk to high surface area activated carbon for energy storage in high performance supercapacitors. *Biomass and Bioenergy*, 144:105909, 2021.

[19] K. Kadirvelu, C. Karthika, N. Vennilamani, and S. Pattabhi. Activated carbon from industrial solid waste as an adsorbent for the removal of rhodamine-b from aqueous solution: Kinetic and equilibrium studies. *Bioresource Technology*, 60(8):1009–1017, 2005.

[20] C. T. Peterson, K. Denniston, and D. Chopra. Therapeutic uses of triphala in ayurvedic medicine. *J Altern Complement Med*, 23(8):607–614, 2017.

[21] J. G. Nirmala, K. Rachineni, S. Choudhary, R. V. Hosur, and M. Lopus. Triphala polyphenols-functionalized gold nanoparticles impair cancer cell survival through induction of tubulin dysfunction. *Journal of Drug Delivary Science and Technology*, 61:102167, 2021.

[22] L. K. Shrestha, S. Shahi, C. L. Gnawali, M. P. Adhikari, R. Rajbhandari, B. P. Pokharel, R. Ma, R. G. Shrestha, and K. Ariga. Phyllanthus emblica seed-derived hierarchically porous carbon materials for high-performance supercapacitor applications. *Materials*, 15:8335, 2022.

[23] F. Xu, J. Yu, T. Tesso, F. Dowell, and D. Wang. Qualitative and quantitative analysis of lignocellulosic biomass using infrared techniques: A mini-review. *Appl. Energy*, 104:801–809, 2013.

[24] A. A. Bamgbola, O. O. Adeyemi, O. O. Olubomehin, A. K. Akinlabi, O. S. Sojinu, and P. O. Iwuchukwu. Isolation and characterization of cellulose from cashew (anacardium occidentale l.) nut shells. *Curr. Res. Green Sustain. Chem.*, 3:100032, 2020.

[25] S. Maji, R. Chaudhary, R.G. Shrestha, R.L. Shrestha, B. Demir, D.J. Searles, J.P. Hill, Y. Yamauchi, K. Ariga, and L.K. Shrestha. High-performance supercapacitor materials based on hierarchically porous carbons derived from artocarpus heterophyllus seed. *ACS Appl. Energy Mater.*, 4(12):12257–12266, 2021.

[26] R.M. Salim, J. Asik, and M.S. Sarjadi. Chemical functional groups of extractives, cellulose and lignin extracted from native leucaena leucocephala bark. *Wood Sci. Technol.*, 55:295–313, 2021.

[27] M. Kruk and M. Jaroniec. Gas adsorption characterization of ordered organic-inorganic nanocomposite materials. *Chem. Mater.*, 13:3169–3183, 2001.

[28] L.K. Shrestha, M. Thapa, R.G. Shrestha, S. Maji, R.R. Pradhananga, and K. Ariga. Rice husk-derived high surface area nanoporous carbon materials with excellent iodine and methylene blue adsorption properties. *CJ.Carbon Res.*, 5:10, 2019.

[29] X. Ma, S. Li, V. Hessel, L. Lin, S. Meskers, and F. Fausto Gallucci. Synthesis of luminescent carbon quantum dots by microplasma process. *Chem. Eng. Process. Process Intensif.*, 140:29–35, 2019.

[30] R.G. Shrestha, S. Maji, A.K. Mallick, A. Jha, R.M. Shrestha, R. Rajbhandari, J.P. Hill, K. Ariga, and L.K. Shrestha. Hierarchically porous carbon from phoenix dactylifera seed for high-performance supercapacitor applications. *Bull. Chem. Soc. Jpn.*, 95:1060–1067, 2022.

[31] Ramesh G Shrestha, Samiran Maji, Lok Kumar Shrestha, and Katsuhiko Ariga. Nanoarchitectonics of nanoporous carbon materials in supercapacitors applications. *Nanomaterials*, 10(4):639, 2020.

[32] Lok Kumar Shrestha, Ramesh G Shrestha, Ratna Chaudhary, Rabindra R Pradhananga, Binita M Tamrakar, Tika Shrestha, Samiran Maji, Roshan L Shretha, and Katsuhiko Ariga. Nelumbo nucifera seed-derived nitrogen-doped hierarchically porous carbons as electrode materials for high-performance supercapacitors. *Nanomaterials*, 11(12):3175, 2021.

[33] Hyun Deog Yoo, Ji-Hyun Jang, Joo-Hyung Ryu, Yong Park, and Seung-Min Oh. Impedance analysis of porous carbon electrodes to predict rate capability of electric double-layer capacitors. *Journal of Power Sources*, 267:411–420, 2014.